Regenerable Sorbents for High-Temperature Desulfurization of Syngas from Biomass Gasification

Jianyu Ma[1], Mehdi Mahmoodinia[1], Kumar R. Rout[2], and Edd A. Blekkan[1,*]

DOI: 10.1002/cite.202000217

In Memory of Prof. Dr.-Ing. Jens Weitkamp

Single-metal high-temperature solid sorbents for syngas cleaning using Mn, Ca, Fe, Cu, or Mo supported on γ-Al_2O_3 were synthesized, characterized, and tested in a fixed-bed reactor. H_2S and SO_2 concentrations in the gas after treatment at T = 400 to 700 °C were compared with thermodynamic calculations. The Mn-based sorbent showed the best ability to achieve a low sulfur residual in the gas, especially at temperatures above 600 °C. Sorbents with Fe, Cu, and Mo gave SO_2 formation in the initial phase, but this could be avoided by a pre-reduction treatment of the sorbent material.

Keywords: High-temperature desulfurization, H_2S concentration, SO_2 formation, Supported metals sorbent

Received: October 08, 2020; *revised:* December 22, 2020; *accepted:* March 03, 2021

1 Introduction

Biomass is a sustainable and renewable source of energy. There are several pathways to convert biomass to more valuable energy forms, including thermochemical methods, biochemical methods, or physical conversion methods [1]. Among these conversion methods, biomass gasification has received considerable attention recently due to its higher overall flexibility and efficiency as well as the mature technologies available for further conversion of the produced syngas [2]. The syngas from biomass gasification is an important energy source and raw material for chemicals synthesis. However, the raw product gas from biomass gasification usually contains several contaminants, including particulate matters, tar, sulfur compounds, nitrogen compounds, etc., which are detrimental to downstream equipment and especially catalysts [3]. Sulfur, which is mainly present in the raw syngas in forms of hydrogen sulfide (H_2S) and sulfur carbonyl (COS), is regarded as the key contaminant, because it is heavily corrosive, toxic to the catalysts, and polluting to the environment [4, 5]. The tolerance of transition metal-catalyzed processes towards sulfur compounds is generally extremely low, hence, detrimental effects of sulfur have been intensively studied. For the cobalt-based Fischer-Tropsch process, the sulfur concentration in the feed gas needs to be lower than 0.1 ppm [6]. It is also reported that the sulfur content should preferably be lower than 0.1 ppm to protect the Cu catalysts involved in the methanol synthesis process [7]. Therefore, sulfur must be thoroughly removed from the syngas prior to being fed into downstream processes. Conventionally, low-temperature sulfur removal methods, which often involve the absorption in solvents, are applied to chemically or physically capture sulfur compounds together with some other impurities [8]. However, the operating temperatures of these methods are usually lower than 100 °C, which induces a significant investment in heat exchange equipment and energy loss for the raw biogas coming from a gasifier in the temperature range of 800 to 900 °C [8, 9], especially when the process layout requires reheating of the gas for further conditioning or processing. Therefore, high-temperature desulfurization with metal oxide-based solid sorbents has received considerable interest because it can efficiently prevent energy loss and reduce investments [10].

High-temperature desulfurization is developed based on the work by Westmoreland and Harrison [11]. The authors conducted a thermodynamic calculation to evaluate the feasibility of metal candidates for high-temperature sulfur removal. They proposed eleven transition metals, i.e., zinc, iron, manganese, molybdenum, vanadium, calcium, strontium, barium, cobalt, copper, and tungsten, as candidates for high-temperature solid sorbents (HTSS). The reactions involved in high-temperature desulfurization with metal oxides are listed as [5]:

[1]Jianyu Ma, Dr. Mehdi Mahmoodinia, Prof. Edd A. Blekkan
edd.a.blekkan@ntnu.no
Department of Chemical Engineering, Norwegian University of Science and Technology (NTNU), 7491 Trondheim, Norway.
[2]Dr. Kumar R. Rout
SINTEF Industry, 7465 Trondheim, Norway.

$$M_xO_y(s) + xH_2S(g) + (y-x)H_2(g) \rightarrow xMS(s) + yH_2O(g) \quad (1)$$

$$MS(s) + H_2O(g) \rightarrow MO(s) + H_2S(g) \quad (2)$$

$$xMS(s) + \left(\frac{y}{2}\right)SO_2(g) \rightarrow M_xO_y(s) + \left(x + \frac{y}{2}\right)S(g) \quad (3)$$

$$xMS(s) + \left(\frac{y}{2}\right)O_2(g) \rightarrow M_xO_y(s) + xSO_2(g) \quad (4)$$

$$MS(s) + 2O_2(g) \rightarrow MSO_4(s) \quad (5)$$

where M stands for metals. Metal oxides can extract H_2S from the gaseous phase through the reaction in Eq. (1) and produce metal sulfide in the solid phase. The produced sulfide can later be regenerated back to oxide states through the reactions involved in Eqs. (2)–(4), depending on the selected regeneration agent. All reactions can occur at medium to higher temperatures, i.e., 400 to 900 °C [4].

Among all the metals proposed by Westmoreland et al. [11], the Ca-, Zn-, Fe-, Cu-, and Mn-based solid sorbents were found to be promising candidates for the desulfurization process [4, 5]. Many efforts have been involved to improve the stability and performance of these solid sorbents, including using different support materials, addition of different promoters, and applying various synthesis methods. Accordingly, sorbents based on these metals show excellent sulfur capture capacity and stability. However, there has been less focus on the residual sulfur levels in the syngas after the desulfurization process, which is crucial for syngas applications. Thermodynamic calculations suggested that copper, zinc, and manganese oxides are favorable for H_2S removal at temperatures lower than 650 °C and can reduce the H_2S concentration to sub-ppm level [12]. However, the reported experimental data for the residual H_2S concentration were divergent, varying from 1 ppm [13–15] up to several hundred ppm [16]. Furthermore, some measurements were restricted by the instrument limitations so that the sulfur residual could not be precisely detected. Therefore, further studies are necessary to investigate the sulfur residue level of the relevant metal oxides and, thereby, their suitability as desulfurization sorbents.

In our previous work, we developed a method to investigate the capacity and stability of sorbent materials and have investigated supported Mn-based sorbents [17]. Furthermore, we have developed and studied a Mo-promoted material with improved properties [18]. Recently, we have introduced a sensitive sulfur analyzer to monitor residual H_2S and SO_2 in the off-gas from the desulfurization reactor at very low concentrations [19]. By measuring the effluent concentrations of H_2S and SO_2 from the sorbent bed, we have also examined the role of the oxide material in forming SO_2 during the initial phases of the sorption cycle, and how pre-reduction of the material can prevent this from occurring.

In this work, we have investigated five different solid sorbents for HTSS (Mn, Ca, Fe, Cu, and Mo metal oxides, all supported on γ-alumina) and compared their properties and ability to reduce the gas-phase sulfur residue level down to the necessary gas purity over a range of relevant temperatures, i.e., 400–700 °C. In addition, we have compared the experimental results with theoretical values from thermodynamic calculations and the formation of SO_2 over calcined sorbent samples.

2 Experimental and Methods

2.1 Chemicals and Materials

Gamma-alumina purchased from Strem Chemicals was used as a support material in the study. The precursors of manganese ($Mn(NO_3)_2{\cdot}4H_2O$), molybdenum ($(NH_4)_6Mo_7O_{24}{\cdot}4H_2O$), copper ($Cu(NO)_2{\cdot}2.5H_2O$), and iron ($Fe(NO)_3{\cdot}4H_2O$) were obtained from Sigma Aldrich. The precursor of calcium ($Ca(NO_3)_2{\cdot}4H_2O$) was obtained from Honeywell Fluka Chemicals.

2.2 Sample Preparation

The desulfurization sorbents used here consist of metal oxides as active phase, supported on γ-alumina as carrier. The support was pre-calcined with air for 10 h at 500 °C and then impregnated with the precursor to synthesize the corresponding metal-based sorbent. After being aged overnight and dried for 24 h under 90 °C, the samples were calcined in air for 5 h in a muffle oven at 700 °C. The calcined samples were crushed and sieved to 150 and 250 µm. The nominal loading of the metal is 15 wt % for all single-metal sorbents and named as 15M, where M represents the metal applied.

2.3 Characterization of Sorbents

The specific surface area of the sorbents according to the BET isotherm as well as the pore diameter and pore volumes were measured with N_2 adsorption at 77 K using a Micromeritics TriStar 3020 instrument. Further details can be obtained in our previous work [17]. We also investigated the crystallinity states of all samples with X-ray powder diffraction on a Bruker AXS D8 Focus diffractometer using CuKα radiation (λ = 1.54 Å). The crystallite size of the active phase was calculated by the Scherrer equation from selected reflections with the shape factor, K, applied as 0.9. The temperature-programmed reduction (TPR) measurements were conducted with a laboratory setup. About 100 mg sample were dried at 130 °C for 30 min under inert gas flow and then cooled down to 100 °C, followed by heating up to 750 °C with a ramp rate of 5 °C min^{-1} under a gas mixture consisting of 7 vol % H_2 in Ar with a gas flow of 50 mL min^{-1} [17].

2.4 Residual Sulfur Concentration Tests

The sorbents, 15Fe, 15Ca, 15Cu, and 15Mo, were first tested for their breakthrough capacities as done previously for the Mn-based sorbent [17, 18]. The tests were performed with a laboratory setup consisting of a gas feeding and metering system, a quartz fixed-bed reactor heated by a furnace, and an analytical section using a quadrupole mass spectrometer (ThermoStar GSD 320 T1 C, MS) to monitor the gas composition. More details can be found in our previous work [17]. 0.2 g of a sorbent was loaded into the reactor and heated up to 600 °C under inert gas (N_2) with a flow rate of 50 mL min^{-1}. Then, the gas mixture (100 mL min^{-1}), containing 40 vol % H_2, 20 vol % N_2, 39.6 vol % Ar, and 0.4 vol % (4000ppm) H_2S, was introduced into the bypass line for 25 min to stabilize the signal in the MS. The sorption was initiated by switching the gas mixture from the bypass line to the reactor line and the composition change of the desulfurized gas exiting the reactor was detected by the MS. The whole desulfurization process was monitored quantitatively based on a regular calibration of the MS signals. The desulfurization capacity of the sorbent before the breakthrough was calculated by the following formula:

$$BC\left(\frac{\text{g of } H_2S}{\text{g of sorbent}}\right) = \frac{Q\int_0^t (C_{in} - C_{out})M_{H_2S}}{V_m \cdot 10^9 m_s} \quad (6)$$

where Q is the flow rate of the model gas, i.e., 100 mL min^{-1}; C_{in} and C_{out} represent the inlet and outlet concentrations of H_2S (ppm), respectively; V_m is the molar volume of gas at 1 atm and 20 °C (24.04 L mol^{-1}), m_s is the mass of the loaded solid sorbent, and M_{H2S} is the molecular weight of H_2S.

For analyzing the residual sulfur concentration, a specific sulfur analyzer was utilized, Thermo Fisher 450i. This analyzer is able to measure the H_2S and SO_2 concentrations in the gaseous phase online with a typical time resolution of 1 min. The upper concentration limitation is 10 ppm for H_2S and 100 ppm for SO_2, which is quite low, and hence, it is critical to know the time passing before the breakthrough, in order to adapt the testing time and protect the analyzer. 0.2 g sorbent was loaded in the reactor and heated up to the desired temperature, i.e., 400, 500, 600, or 700 °C, under inert gas (N_2) with a flow rate of 50 mL min^{-1}. The sorbent 15Mn went through a slightly different heating process, which was the same as that used for the desulfurization capacity and stability test, i.e., heating to 600 °C under 50 mL min^{-1} 50 vol % H_2/N_2 gas flow and keeping for 1 h, then changing the temperature to the desired sorption temperature. Then, the model gas was introduced into the reactor to start the sulfur residue test. A lower feeding H_2S concentration (compared to the capacity measurements) was applied to prolong the time before the breakthrough and ensure the collection of enough data points. A gas mixture (100 mL min^{-1}) of 40 vol % H_2, 20 vol % N_2, 19.8 vol % Ar, and 0.2 vol % (2000 ppm) H_2S was fed to the reactor with the solid sorbent, and the off-gas was analyzed by the sulfur analyzer. To avoid exposing the instrument to sulfur concentrations above the upper limit, the measurement was terminated once a sudden increase of the sulfur concentration was observed or when the experiment had lasted 40 min. With this setup, the sulfur content can be measured precisely down to approximately 100 ppb. Depending on the capacity of the sorbent used, the measurements usually lasted for 15–40 min. The gas was diluted with synthetic air by a volume factor of 5 before entering the analyzer, and the concentrations of SO_2 or H_2S are calculated by the following equation:

$$RC_s(\text{ppm}) = 5RC_D \quad (7)$$

where RC_s is the concentration in the off-gas and RC_D is the observed value from the analyzer. The lowest attainable sulfur levels were obtained by establishing steady state in the sulfur residue state and calculating the average values. The steady state is defined according to the H_2S concentration curves and defined as 10 continuous minutes with the lowest average H_2S and SO_2 concentrations.

2.5 Thermodynamic Calculations

The theoretical residual sulfur concentration in the gas phase at equilibrium was also calculated for the tested metal oxides using FactSage. The systems investigated were MnO, Fe_2O_3, FeO, CuO, MoO_2, MoO_3, and CaO as well as another commonly used metal oxide for desulfurization, ZnO. The input gas composition is defined as 40 vol % H_2, 0.2 vol % H_2S, 40 vol % N_2, and 19.8 vol % Ar, which is the same as the gas mixture used for the sulfur residue test, and the amount ratio of gaseous and solid species were both defined as 1 mol. Calculations were performed for temperatures in the range of 400–1000 °C. The calculated equilibrium levels of sulfur compounds, both for H_2S and SO_2, are presented in Figs. 1a and b, respectively. As shown in Fig. 1 a, the residual H_2S levels for all metal oxides increase with temperature, which is expected since sulfidation is an exothermic reaction. The H_2S residue levels for Fe_2O_3, FeO, and MoO_2 are above 100 ppm at temperatures higher than 540, 590, and 730 °C, respectively, which are higher than for the other metal oxides and render these materials less suitable for HTSS. Other metal oxides exhibit excellent H_2S sorption (< 10 ppm) performances at temperatures lower than 770 °C, declining in this order: MnO > CaO > ZnO > CuO. The H_2S residual levels on the CaO and MnO solid sorbents increase gradually with temperature and reach 11.2 and 5.8 ppm at 1000°C, respectively, while for ZnO it increases sharply at temperatures above 800 °C (Fig. 1a). There is almost no residual H_2S over CuO and MoO_3, and this is also not affected by temperature, but as shown in Fig. 1b, the SO_2 concentrations at equilibrium are remarkably high over CuO and MoO_3, indicating that H_2S can be converted to SO_2 in this temperature range over CuO and

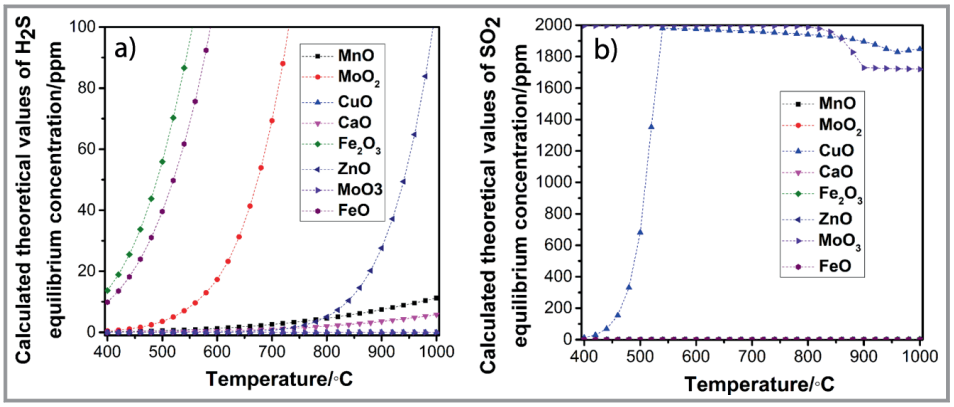

Figure 1. Theoretically calculated equilibrium sulfur concentrations in the gas phase with different metal oxides, i.e., MnO, Fe_2O_3, CuO, MoO_2, ZnO, MoO_3, FeO, and CaO, at temperatures from 400 to 1000 °C. a) H_2S, b) SO_2.

MoO_3, while the metal oxides are reduced. All the other metals show little tendency to convert H_2S to SO_2. Our findings on these metal oxides are in agreement with the literature [4, 5].

Westmoreland et al. [20] proposed that the maximum temperature applied for zinc oxide should be below 600 °C, due to the vaporization issue. The thermodynamic calculation results also suggest a high content of Zn vapor when the temperature is higher than 600 °C. Normally, iron or titanium is added as a promoter to inhibit zinc vaporization by forming zinc ferrite or zinc titanate [13, 21]. In this study, the desulfurization performance of the single metal-based sorbents is compared at temperatures in the range of 400 to 700 °C. Hence, zinc oxide was excluded from the experimental study.

3 Result and Discussion

3.1 Sample Characterization Results

3.1.1 N_2 Adsorption Measurement

The textural properties of all fresh sorbents are shown in Tab. 1. The surface area of the alumina support was measured to be 169 m^2g^{-1} with an average pore width of 12.7 nm and a pore volume of 0.61 cm^3g^{-1}. The surface areas of the samples decreased to different degrees, however, most of them are similar, in the range from 121 to 140 m^2g^{-1}. The 15Ca and 15Mo solid sorbents had even lower surface areas, 72 and 104 m^2g^{-1}, respectively. These two samples also had slightly larger average pore widths (18.0–18.3 nm), compared to 12.8–14.1 nm for the other samples. The pore volume was similar for all samples, in the range of 0.44–0.66 cm^3g^{-1}.

3.1.2 X-ray Diffraction Measurement

The XRD patterns of all fresh (calcined) samples are shown in Fig. 2. The diffraction pattern of 15Mn (A) indicates that Mn_2O_3 is the dominant phase of Mn in the 15Mn solid sorbent after thermal treatment in air. The diffractions at 2θ

Table 1. Textural properties of all fresh sorbents as obtained from N_2 sorption measurement.

Sorbent	Surface area [m^2g^{-1}]	Average pore width [nm]	Pore volume [cm^3g^{-1}]
γ-Al_2O_3	169	12.7	0.61
15Mn	121	14.1	0.47
15Fe	131	12.8	0.57
15Cu	140	13.8	0.66
15Mo	104	18.3	0.61
15Ca	72	18.0	0.44

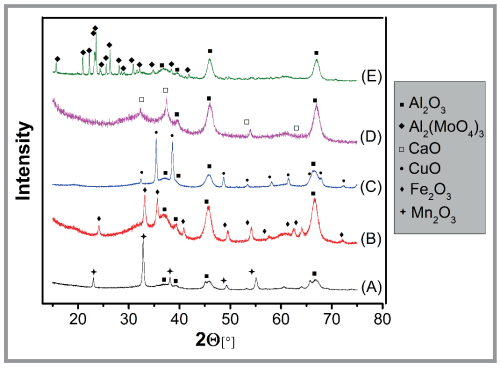

Figure 2. XRD patterns for all sorbents. A) 15Mn, B) 15Fe, C) 15Cu, D) 15Ca, E) 15Mo.

values of 24, 33, 36, 41, 49.5, 54, 58, 62.5, and 64.5° in the pattern of 15Fe (B) are attributed to iron(III) oxide (Fe_2O_3), and the sharp peaks indicate a high degree of crystallinity of the active phase. In the pattern of 15Cu (C), the sharp characteristic peaks at 2θ values of 35.5 and 38.5°, along with other low-intensity peaks, indicate the presence of tenorite (CuO). The diffraction pattern of 15Ca (D) shows three characteristic peaks of CaO at the 2θ values of 32.5, 37.5, and 54°. All active phases existing on the sorbents are present as metal oxides, however, the main active phase detected on the 15Mo sample (E) is aluminum molybdate. This indicates a strong interaction between Mo and γ-alumina, and

the sharp peaks at 2θ values of 21, 22.5, and 25.5° are evidence of high crystallinity of the binary phase. However, aluminum molybdate ($Al_2(MoO_4)_3$) can be regarded as a combination of Al_2O_3 and MoO_3. In this study, more attention will be paid to the phenomena related to the chemical composition of the sorbent not the bonding relationship between the active phase and the support. Hence, in the latter part, the active phase of 15Mo will be considered to be MoO_3.

The crystallite sizes were obtained by using the Scherrer equation. The calculated crystallite sizes of all species on the sorbents and the selected positions of the corresponding characteristic peaks are listed in Tab. 2. The particle sizes of Mn_2O_3, Fe_2O_3, and CuO are between 20 and 30 nm. The size of CaO is larger (38 nm), and the $Al_2(MoO_4)_3$ particle is the largest (64 nm).

3.1.3 Temperature-Programmed Reduction

The reducibility of the samples was investigated by temperature-programmed reduction (TPR) in the temperature range of 100 to 750 °C using diluted hydrogen (7 vol % in Ar). The resulting TPR profiles are shown in Fig. 3. The TPR profile for the 15Ca-Al_2O_3 sorbent (curve A) illustrates very low reducibility. Two very low-intensity reduction peaks at 500 and 600 °C are most probably due to impurities in the Ca precursor or in the support material since the CaO is not expected to be reduced at these conditions. The XRD patterns in Fig. 2 (cure A) revealed that the dominant Mn phase in the sorbent 15Mn is Mn_2O_3, and therefore, a stepwise reduction is expected: $Mn_2O_3 \rightarrow Mn_3O_4 \rightarrow MnO$ [22]. The TPR profile of 15Mn (curve B) confirms this, as two peaks were observed, one at approximately 336 °C, corresponding to the reduction of Mn_2O_3 to Mn_3O_4, and the other peak at 420 °C, corresponding to the reduction of Mn_3O_4 to MnO. The sharp peak at 255 °C in the TPR profile of 15Cu (curve C) indicates that CuO is much easier to reduce and that metallic Cu is formed. Although these results have not been quantified, the sample size and scale of the profiles are comparable, confirming the high reducibility of supported Cu. The observed profile is in good agreement with other studies [23, 24]. It has also been reported that the reduction behavior of Cu-based catalysts may be different at higher Cu loadings (higher than 10 wt %) with high dispersion, and TPR profiles with two reduction peaks have been reported [25]. The single peak observed here could indicate a rather poor dispersion of Cu on the support. The TPR profile for the 15Mo sorbent is rather more complex, with two broad peaks at 430 and 571 °C and a small shoulder at approx. 540 °C (curve D). This indicates the range of oxidation states possible in this metal oxide [26, 27]. Combining the TPR results with XRD, it can be proposed that the main Mo-containing compound on the sorbent is $Al_2(MoO_4)_3$, representing Mo^{6+}. The two main reduction peaks in the TPR curve suggest that the reduction happens through two steps, i.e., $Mo^{6+} \rightarrow Mo^{5+} \rightarrow Mo^{4+}$, possibly with some further reduction to Mo^{2+}. Hence, it can be deduced that Mo is present as MoO_2 following a reduction in the sorption experiment (600 °C in H_2). The 15Fe sample (curve E) exhibits one main broad reduction peak starting at 230 °C and peaking at 438 °C, probably linked with the reduction of Fe_2O_3 to Fe_3O_4. There are also broad and weak peaks at higher temperatures, around 550 and 650 °C, indicating that further reduction to Fe(II) and metallic Fe is possible but incomplete also in the TPR experiment.

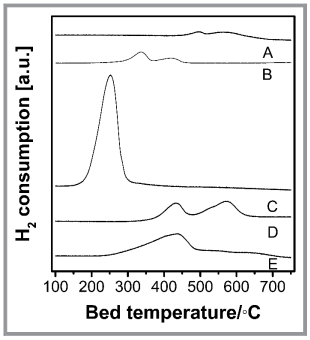

Figure 3. TPR profiles of all sorbents. A) 15Ca, B) 15Mn, C) 15Cu, D) 15Mo, E) 15Fe.

3.2 Evaluation of Desulfurization Capacities of the Sorbents

Desulfurization performance tests were carried out on all sorbents to evaluate the breakthrough capacities and also to predict when the breakthrough will happen in order to protect the analytical sulfur analyzer. All materials behave in a similar fashion: first, the H_2S signal in the mass spectrometer declines sharply from the highest level (input gas level) during the stabilization step to the lowest level and then stabilizes for some time, depending on the sorbent's capacity. The capacities of these samples are listed in Tab. 2. It is worth mentioning that the sorption processes also produced more water, which was detected but not quantified in the MS for sorbents 15Mo, 15Fe, and 15Cu. The amount of

Table 2. Crystallite sizes of species of all sorbents calculated from XRD by the Scherrer equation.

Sorbent Code	15Mn	15Fe	15Cu	15Ca	15Mo
Active phase	Mn_2O_3	Fe_2O_3	CuO	CaO	$Al_2(MoO_4)_3$
Characteristic peak position (2θ) [°]	33	54	49	25	26.5
Crystallite size [nm]	27	21	30	38	64

water initially increased and was stable for several minutes (approx. 4 min for 15Fe and 15Cu, 8 min for 15Mo sorbent), and subsequently decreased to a lower, stable level. This confirms the reducibility of the active phases of these sorbents, as also observed in the TPR experiments. The capacities of these single metal-based sorbents at 600 °C at these conditions are reported in Tab. 3 and decline in the following order: 15Mn > 15Fe > 15Mo > 15Cu > 15Ca.

Table 3. Desulfurization capacities of the sorbents at 600 °C under a gas mixture consisting of 0.4, 39.6, 40.0, and 20 vol % for H_2S, Ar, H_2, and N_2, respectively.

Sorbent	Capacity [$g_{H2S}g_{sorbent}^{-1}$]
15Mn	0.064
15Fe	0.056
15Cu	0.025
15Mo	0.050
15Ca	0.018

3.3 Residual Sulfur Concentrations on Mn-based Sorbent

The 15Mn sorbent was pre-reduced as described in Sect. 2.4, and as discussed in the TPR section, it is assumed that Mn_2O_3 was reduced to MnO during pre-reduction. The measured residual H_2S concentration for the 15Mn solid sorbent at different temperatures are presented in Fig. 4a. There are some fluctuations at the beginning of the measurements, but after a few minutes, the detected levels are low and relatively stable. The H_2S residual concentrations at the steady state measured at 400, 500, and 600 °C were similar (0.16 to 0.22 ppm) and lower than the observed residual level at 700 °C (0.92 ppm) (Fig. 4c). The breakthrough occurred after 27 min at 400 °C, and after 37 min at 500 °C, respectively, at higher temperatures, the experiment was stopped before the breakthrough occurred. The duration before the breakthrough reflects the capacity of the sorbent, and these findings are in agreement with previous studies indicating that the capacity of the Mn-based sorbents increases with increasing temperature [28–30].

As mentioned before, there are also traces of SO_2 in the gas phase. Over 15Mn, the concentration is very low, during the stable phase of the cycle, the concentration stayed below 0.08 ppm. We proposed two mechanisms for SO_2 formation during the high-temperature desulfurization process in our previous study [19], one is through sulfate decomposition and the other is through H_2S oxidation by metal oxides with higher oxidation states. A very low SO_2 concentration from the pre-reduced 15Mn solid sorbent, especially at the beginning of the sorption, confirms that in this case the second mechanism is important. However, it is notable that the overall measured SO_2 residual concentrations at all temperatures are higher than their corresponding theoretical calculated values (Fig. 1b). This might be due to the reaction between H_2S and traces of Mn_2O_3 due to insufficient reduction. The average effluent SO_2 levels were in the range of 0.01–0.06 ppm for all temperatures (Fig. 4c).

3.4 Residual Sulfur Concentrations on Ca-based Sorbent

The Ca-based solid sorbent had the shortest pre-breakthrough time of all tested samples, which corresponds to the lowest capacity (Tab. 1), especially at 400 °C where only four valid data points were captured (Fig. 5a). Similar to 15Mn, the capacities of 15Ca increased with increasing temperature, but in addition, the profiles were less stable. The measured residual H_2S at 700 °C was in the range of 2.5 to 5.4 ppm, higher than at lower temperatures, here, the concentration exhibits a clear maximum after 8 min and a minimum after 16 min. The H_2S level at 600 °C was lower than that at 500 °C, which is again unexpected in light of the

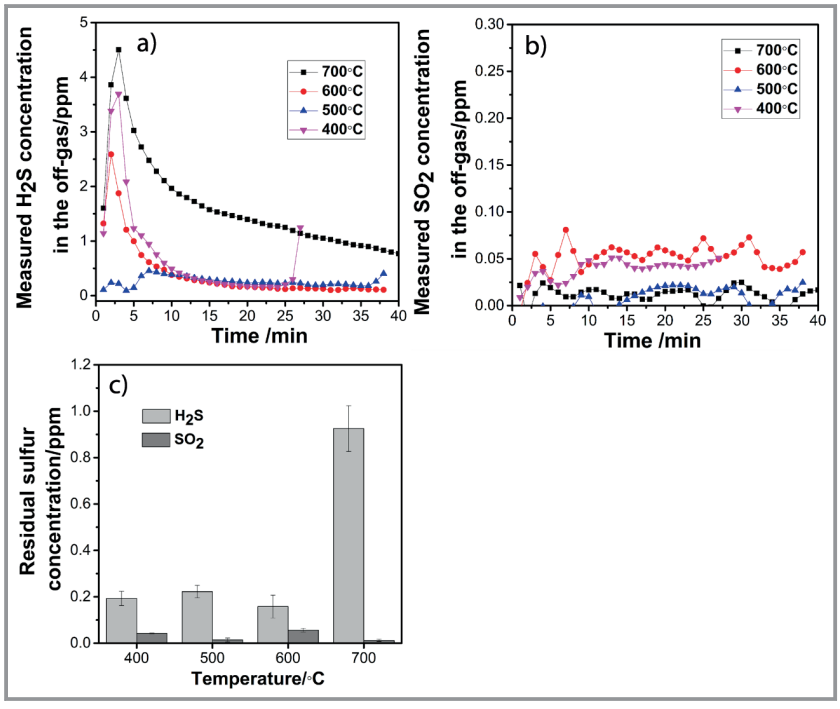

Figure 4. Measured sulfur residual gas-phase concentrations at different temperatures for the 15Mn sorbent. a) H_2S residual, b) SO_2 residual, c) average values of H_2S and SO_2 residual during steady state.

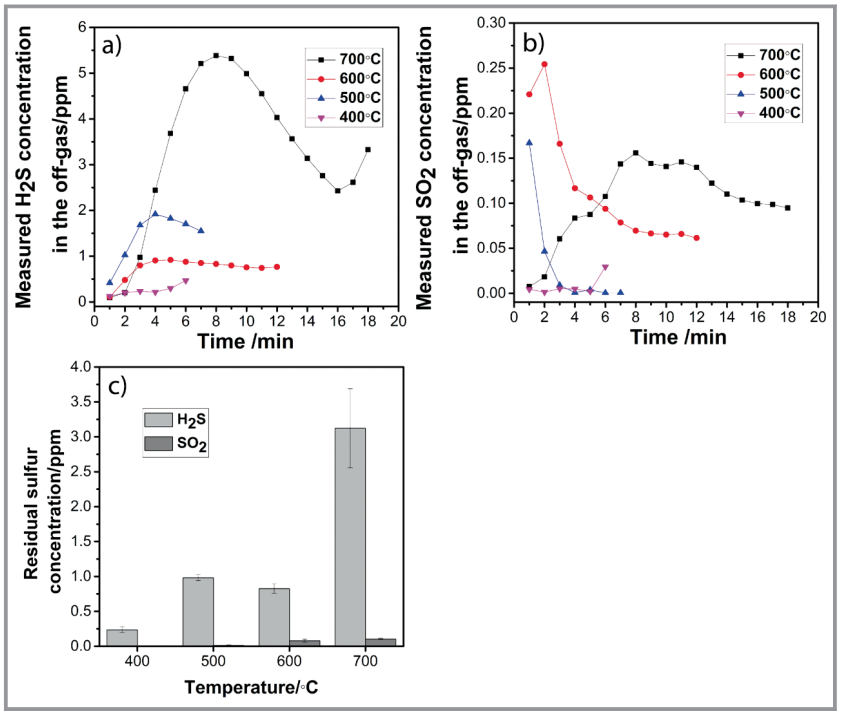

Figure 5. The measured sulfur residual gas-phase concentrations at different temperatures for the 15Ca sorbent. a) H_2S residual, b) SO_2 residual, c) average values of H_2S and SO_2 residual during steady state.

thermodynamic relations (Fig. 1a). SO_2 formation was very low over 15Ca. This is in agreement with the TPR of this sample, showing a very limited reducibility (Fig. 3).

The average minimum values shown in Fig. 4c are very low, but it is worth taking into account that the capacity is low and that it was difficult to obtain a steady-state situation where good measurements could be performed. Calcium-based sorbents have been reported to be promising for high-temperature desulfurization, for either in situ or downstream use [5]. However, the most applied Ca-based materials are minerals like dolomite or limestone, which are unsupported and, thus, contain more active material per total mass unit [30–33].

3.5 Residual Sulfur Concentrations on Fe-based Sorbent

The measured residual H_2S concentration results for the Fe-based sorbent are presented in Fig. 6a. Similar to the Mn-based sorbent, there are some fluctuations at the beginning of the measurements, which were stabilized after 10 min. The H_2S level was higher at 700 °C than at lower temperatures during the stable period after 10 min. Significant SO_2 formation was observed at the beginning of the sorptions at all temperatures, but this decreased rapidly to stable low levels after around 5 min. The main compound on the support of the sorbent 15Fe, according to the XRD patterns, was Fe_2O_3, which can be reduced to FeO under the reducing environment [16].

The lowest attainable values of residual H_2S and SO_2 of all temperatures are given in Fig. 6c. The stable concentrations of SO_2 decrease with increasing temperatures in the range of 400–600 °C, but the peak level during the initial perturbation is higher for higher temperatures, indicating a limited amount of reducible oxide and possibly a kinetic influence on the shape of the curve. This is confirmed by the experiment shown in Fig. 6d, where a pre-reduced 15Fe sample

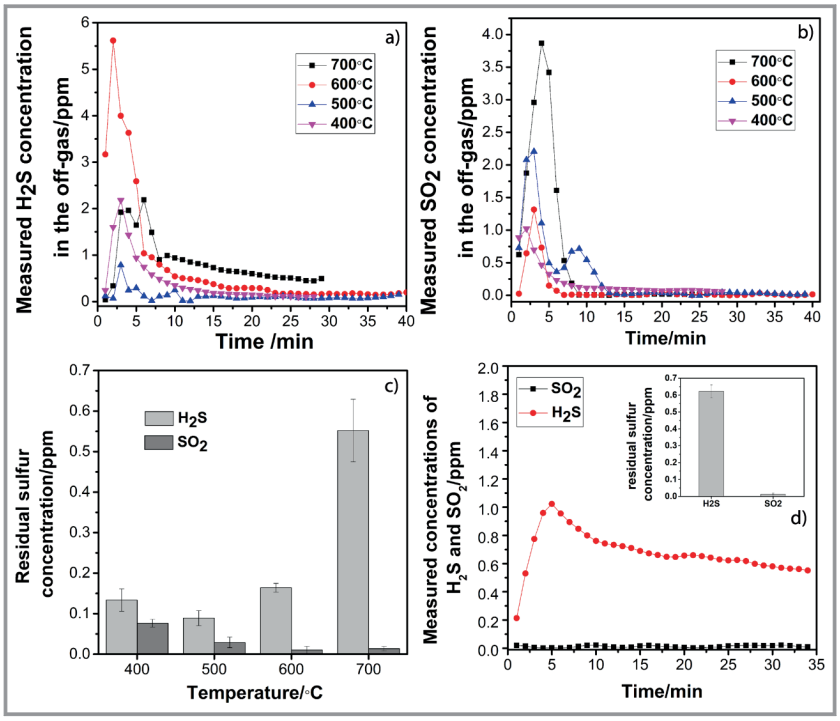

Figure 6. Measured sulfur residual gas-phase concentrations at different temperatures for the 15Fe sorbent. a) H_2S residual, b) SO_2 residual, c) average values of H_2S and SO_2 residual during steady state, d) sorbent with pre-reduction treatment (both pre-reduction and sorption at 600 °C).

(pre-reduced at 600 °C under a gas flow of 40 vol % H_2 in N_2 for 10 min), underwent a sulfur residue test at 600 °C. Following reduction, virtually no SO_2 was detected, indicating the role of Fe_2O_3 in SO_2 formation. However, the stable value for residual H_2S was 0.62 ppm, which is higher than in the case without pre-reduction.

3.6 Residual Sulfur Concentrations on Cu-based Sorbent

The behavior of the 15Cu sorbent is shown in Fig. 7. The period before the breakthrough for the 15Cu sorbent is much shorter compared to the Mn- and Fe-based sorbents, under all tested temperatures. This might be due to the reduction of copper oxide to elementary copper at higher temperatures, combined with sintering of the active phase [34]. After the initial peak, the H_2S curves reached steady state after around 10 min (Fig. 7a), and the expected temperature response on the stable level was observed. The stable low level was below 1 ppm up to 700 °C (Fig. 7c). SO_2 formation was apparent at the beginning of the measurement, which demonstrates the conversion of H_2S to SO_2 by copper oxides. Theoretical calculations confirm that copper oxides are more reducible than the other oxides studied here, and thus, have a stronger ability to convert H_2S to SO_2. The average SO_2 residue levels under Cu-based solid sorbents are shown in Fig. 7c, passing through a maximum at 600 °C.

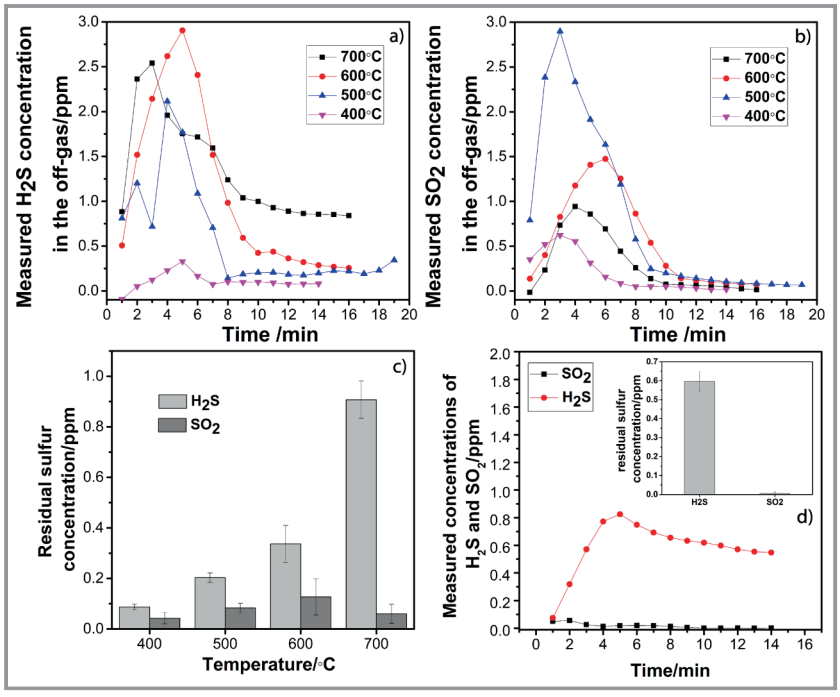

Figure 7. Measured sulfur residual gas-phase concentrations at different temperatures for 15Cu sorbent. a) H_2S residual, b) SO_2 residual, c) average values of H_2S and SO_2 residual during steady state, d) sorbent with pre-reduction treatment (both pre-reduction and sorption at 600 °C).

Fig. 7d shows the sorption experiment at 600 °C following the same pre-reduction protocol as described for 15Fe. Pre-reduction virtually eliminated SO_2 formation, but also led to a slightly higher H_2S level at steady state (0.60 ppm vs 0.34 ppm). The reducibility of the Cu-based sorbent is considered less ideal for this application concerning sulfur capture capacity [5], and studies have been conducted to avoid CuO reduction by adding promoters [35, 36] or using suitable support materials [37, 38] to increase their efficiency. Reduction by H_2S can be considered to occur according to Eqs. (8) and (9) [34], and metallic Cu adsorbs H_2S according to Eq. (10) [16].

$$3CuO + H_2S \rightleftharpoons 3Cu + SO_2 + H_2O \quad (8)$$

$$3Cu_2O + H_2S \rightleftharpoons 6Cu + SO_2 + H_2O \quad (9)$$

$$2Cu + H_2S \rightleftharpoons Cu_2S + H_2 \quad (10)$$

3.7 Residual Sulfur Concentrations on Mo-based Sorbent

The results of residual sulfur tests on sorbent 15Mo are shown in Fig. 8. The period before breakthrough at 400 °C was shorter than at the other temperatures, however, with a very low H_2S residual level. The H_2S residual levels increased with increasing temperature, staying below 1 ppm up to 600 °C (Fig. 8a). SO_2 formation was only detectable at temperatures of 500 °C and above (Fig. 8b), and the values were very low at steady state. The absence of SO_2 formation at the lowest temperature is surprising since the material was partly reducible in TPR at temperatures below 400 °C. This could indicate that the proposed Al-Mo compound ($Al_2(MoO_4)_3$) is less reactive towards H_2S.

The H_2S average residual values at steady state increased with increasing temperature but were below 1 ppm up to 600 °C (Fig. 8c). The maximum SO_2 concentration (both in terms of peak value and steady-state level) was observed at 500 °C, confirming a more complex behavior of this material. Also, for 15Mo pre-reduction of the material at 600 °C eliminated SO_2 formation (Fig. 8d). But in this case, the H_2S residual was also lower for the reduced sample.

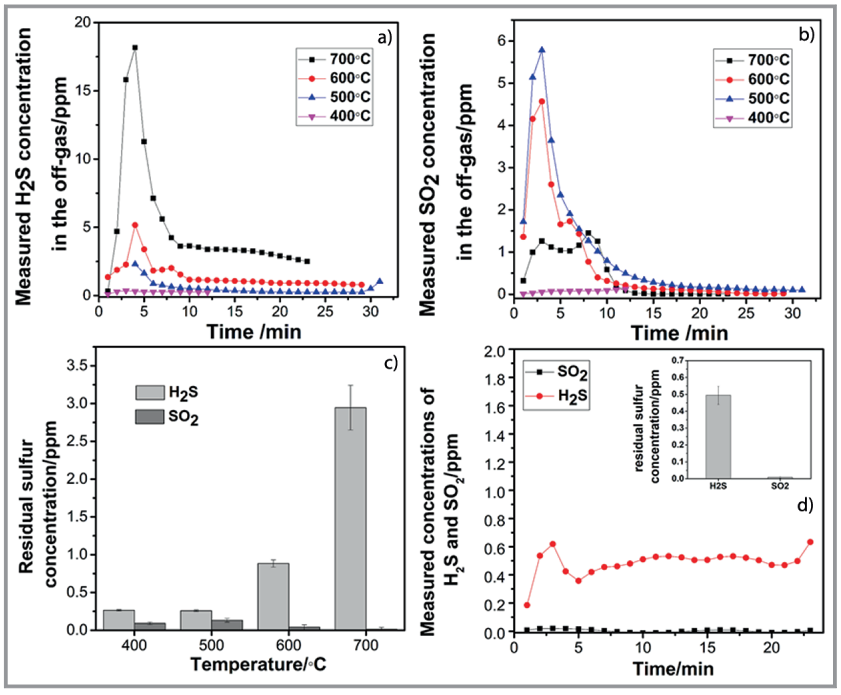

Figure 8. Measured sulfur residual gas-phase concentrations at different temperatures for 15Mo sorbent. a) H_2S residual, b) SO_2 residual, c) average values of H_2S and SO_2 residual during steady state, d) sorbent with pre-reduction treatment (both pre-reduction and sorption at 600 °C).

4 Summary and Discussion

To summarize and compare the lowest attainable residual H_2S and SO_2 concentrations with the theoretical values, all single-metal sorbents exhibited lower residual H_2S levels at all tested temperatures comparing with corresponding values from thermodynamic calculations. This is probably because the thermodynamic calculations are done for a batch situation with a set number of moles of the species and cannot reflect the experimental system where the fixed bed provides several cleaning stages from the entry to the exit of the bed. The H_2S levels at 600 °C decreased in the order 15Mo > 15Ca > 15Cu > 15Fe > 15Mn, i.e., they do not follow the order shown in Fig. 1a. This could be due to slightly different ratios (calculations were done for 1 mol of metal oxide, experimentally the weight-loadings were the same), and in some cases, the sorption stoichiometry is different. The sorbents also have different physical properties, such as specific area and porosity, and the active phases have different particle sizes, all of which may kinetically influence the sorption reaction. Hence, deviations from the predicted values are not surprising. The formation of SO_2 is a practical issue that will influence the design and operation of a cleaning stage based on these sorbents. But this phenomenon also provides some insight into the behavior of the material during early stages of the sorption process. It can be noted that for the sorbents 15Fe, 15Cu, and 15Mo, pre-reduction suppressed the initial SO_2 formation, demonstrating the importance of the reducibility of the metal oxide and providing a practical solution to the issue of SO_2 formation if the sorbents are applied in an industrial process. But the effect of the pre-reduction on the stable residual level (the ability of the material to provide a sufficiently clean gas) should also be noted, the effect was negative on the sorbents 15Fe and 15Cu, while it was positive on 15Mo.

5 Conclusion

In this study, five single-metal sorbents, namely, 15Mn, 15Ca, 15Fe, 15Cu, and 15Mo, all supported on gamma-alumina were prepared and the lowest residual gas-phase sulfur concentrations (H_2S and SO_2) in a model syngas after being exposed to single-metal sorbents in a fixed-bed, continuous reactor at different temperatures, were recorded and compared to thermodynamical calculations. In terms of the residual sulfur level during steady state, Fe-, Mn- and Cu-based sorbents showed better performance than 15Ca and 15Mo, and H_2S residual concentration was found to be below 1 ppm over the whole temperature range of 400 to 700 °C at the investigated conditions. The Ca- and Mo-based sorbent can also eliminate H_2S to lower than 1 ppm, but only at temperatures up to 600 °C. The formation of SO_2 during the initial stages of sorption was also investigated. When it comes to SO_2 formation, this is strongly linked with the reducibility of the sorbents and is not an important issue for Ca-based sorbents. For the other sorbents, a pre-reduction step significantly reduced or eliminated this issue, confirming that the main route is through oxidation of sulfur by the metal oxides and simultaneous reduction of the metal oxide to a lower oxidation state.

The Norwegian Research Council is gratefully acknowledged for financial support through contracts 267986 and 257622.

References

[1] X. M. Meng, *Biomass Gasification: The Understanding of Sulfur, Tar, and Char Reaction in Fluidized Bed Gasifiers*, Ph.D. Thesis, TU Delft **2012**.

[2] G. Ruoppolo, P. Ammendola, R. Chirone, F. Miccio, *Waste Manage.* **2012**, *32 (4)*, 724–732. DOI: https://doi.org/10.1016/j.wasman.2011.12.004

[3] S. C. Tseng, S. S. Tamhankar, C. Y. Wen, *Chem. Eng. Sci.* **1981**, *36 (8)*, 1287–1294. DOI: https://doi.org/10.1016/0009-2509(81)80163-7

[4] S. Cheah, D. L. Carpenter, K. A. Magrini-Bair, *Energy Fuels* **2009**, *23 (11)*, 5291–5307. DOI: https://doi.org/10.1021/ef900714q

[5] X. Meng, W. De Jong, R. Pal, A. H. M. Verkooijen, *Fuel Process. Technol.* **2010**, *91 (8)*, 964–981. DOI: https://doi.org/10.1016/j.fuproc.2010.02.005

[6] H. Boerrigter, H. D. Uil, H. P. Calis, Green Diesel from Biomass via Fischer-Tropsch Synthesis: New Insights in Gas Cleaning and Process Design, *Pyrolysis and Gasification of Biomass and Waste, Expert Meeting*, Strasbourg, September **2002**.

[7] H. H. Kung, *Catal. Today* **1992**, *11 (4)*, 443–453. DOI: https://doi.org/10.1016/0920-5861(92)80037-N

[8] P. J. Woolcock, R. C. Brown, *Biomass Bioenergy* **2013**, *52*, 54–84. DOI: https://doi.org/10.1016/J.BIOMBIOE.2013.02.036

[9] N. Abdoulmoumine, S. Adhikari, A. Kulkarni, S. Chattanathan, *Appl. Energy* **2015**, *155*, 294–307. DOI: https://doi.org/10.1016/j.apenergy.2015.05.095

[10] A. H. Lillebø, A. Holmen, B. C. Enger, E. A. Blekkan, *Wiley Interdiscip. Rev.: Energy Environ.* **2013**, *2 (5)*, 507–524. DOI: https://doi.org/10.1002/wene.69

[11] P. R. Westmoreland, D. P. Harrison, *Environ. Sci. Technol.* **1976**, *10 (7)*, 659–661. DOI: https://doi.org/10.1021/es60118a010

[12] X. Meng, W. De Jong, A. H. M. Verkooijen, *Environ. Prog. Sustainable Energy* **2009**, *28 (3)*, 360–371. DOI: https://doi.org/10.1021/es60118a010

[13] R. Gupta, S. K. Gangwal, S. C. Jain, *Energy Fuels* **1992**, *6 (1)*, 21–27. DOI: https://doi.org/10.1021/ef00031a004

[14] N. O. Ikenaga, Y. Ohgaito, H. Matsushima, T. Suzuki, *Fuel* **2004**, *83 (6)*, 661–669. DOI: https://doi.org/10.1016/j.fuel.2003.08.019

[15] M. Kobayashi, H. Shirai, M. Nunokawa, *Powder Technol.* **2008**, *180 (1–2)*, 178–183. DOI: https://doi.org/10.1016/j.powtec.2007.03.027

[16] G. Sick, K. Schwerdtfeger, *Metall. Trans. B* **1987**, *18 (3)*, 603–609. DOI: https://doi.org/10.1007/bf02654274

[17] S. Chytil, M. Kure, R. Lødeng, E. A. Blekkan, *Fuel* **2017**, *196*, 124–133. DOI: https://doi.org/10.1016/j.fuel.2017.01.087

[18] J. Ma, K. R. Rout, M. Sauer, M. Mahmoodinia, E. A. Blekkan, *Biomass Bioenergy* **2020**, *143*, 105843. DOI: https://doi.org/10.1016/j.biombioe.2020.105843

[19] J. Ma, M. Mahmoodinia, K. R. Rout, E. A. Blekkan, *High-Temperature Desulfurization by Mn-Mo Sorbent: An Investigation on Optimal Regeneration Condition and Prevention of SO_2 Formation*, in preparation.

[20] P. R. Westmoreland, J. B. Gibson, D. P. Harrison, *Environ. Sci. Technol.* **1977**, *11 (5)*, 488–491. DOI: https://doi.org/10.1021/es60128a007

[21] S. Lew, M. Flytzani-Stephanopoulos, A. F. Sarofim, *Mechanistic and Kinetic Studies of High-Temperature Coal Gas Desulfurization Sorbents*, Report, No. DOE/PC/88927-12, Massachusetts Institute of Technology, Cambridge, MA **1991**. DOI: https://doi.org/10.2172/6166792

[22] E. R. Stobbe, B. A. De Boer, J. W. Geus, *Catal. Today* **1999**, *47 (1–4)*, 161–167. DOI: https://doi.org/10.1016/S0920-5861(98)00296-X

[23] M. F. Luo, Y. J. Zhong, X. X. Yuan, X. M. Zheng, *Appl. Catal., A* **1997**, *162 (1–2)*, 121–131. DOI: https://doi.org/10.1016/S0926-860X(97)00089-6

[24] C. S. Chen, W. H. Cheng, S. S. Lin, *Appl. Catal., A* **2003**, *238 (1)*, 55–67. DOI: https://doi.org/10.1016/S0926-860X(02)00221-1

[25] W. P. Dow, Y. P. Wang, T. J. Huang, *Appl. Catal., A* **2000**, *190 (1–2)*, 25–34. DOI: https://doi.org/10.1016/S0926-860X(99)00286-0

[26] H. Liu, Y. Xu, *Chin. J. Catal.* **2006**, *27 (4)*, 319–323. DOI: https://doi.org/10.1016/s1872-2067(06)60020-x

[27] J. Park, J. Kim, H. Lee, *Bull. Korean Chem. Soc.* **1998**, *19 (12)*, 1363–1368.

[28] W. J. W. Bakker, F. Kapteijn, J. A. Moulijn, *Chem. Eng. J.* **2003**, *96 (1–3)*, 223–235. DOI: https://doi.org/10.1016/j.cej.2003.08.022

[29] L. F. Guo, K. L. Pan, H. M. Lee, M. B. Chang, *Ind. Eng. Chem. Res.* **2015**, *54 (44)*, 11040–11047. DOI: https://doi.org/10.1021/acs.iecr.5b02078

[30] J. Zhang, Y. Wang, D. Wu, *Energy Convers. Manage.* **2003**, *44 (3)*, 357–367. DOI: https://doi.org/10.1016/S0196-8904(02)00068-7

[31] R. Álvarez-Rodríguez, C. Clemente-Jul, *Fuel* **2008**, *87 (17–18)*, 3513–3521. DOI: https://doi.org/10.1016/j.fuel.2008.07.010

[32] Z. Luo, C. Yin, X. Li, M. Fang, X. Gao, J. Zhou, M. Ni, K. Cen, *Energy* **1997**, *22 (11)*, 1051–1058. DOI: https://doi.org/10.1016/S0360-5442(97)00036-4

[33] J. Wang, J. Guo, R. Parnas, B. Liang, *Fuel* **2015**, *154*, 17–23. DOI: https://doi.org/10.1016/j.fuel.2015.02.105

[34] T. Kyotani, H. Kawashima, A. Tomita, A. Palmer, E. Furimsky, *Fuel* **1989**, *68 (1)*, 74–79. DOI: https://doi.org/10.1016/0016-2361(89)90014-8

[35] Z. Li, M. Flytzani-Stephanopoulos, *Ind. Eng. Chem. Res.* **1997**, *36 (1)*, 187–196. DOI: https://doi.org/10.1021/ie960245d

[36] L. D. Gasper-Galvin, A. T. Atimtay, R. P. Gupta, *Ind. Eng. Chem. Res.* **1998**, *37 (10)*, 4157–4166. DOI: https://doi.org/10.1021/ie930439i

[37] Z. Ozaydin, S. Yasyerli, G. Dogu, *Ind. Eng. Chem. Res.* **2008**, *47 (4)*, 1035–1042. DOI: https://doi.org/10.1021/ie071039g

[38] O. Karvan, H. Atakül, *Fuel Process. Technol.* **2008**, *89 (9)*, 908–915. DOI: https://doi.org/10.1016/j.fuproc.2008.03.004

